Fault Tolerance with Bare Ancillary Qubits for a $[[7, 1, 3]]$ Code

Muyuan Li, Mauricio Gutiérrez, Stanley E. David, Alonzo Hernandez, and Kenneth R. Brown*
Schools of Computational Science and Engineering; Chemistry and Biochemistry; and Physics
Georgia Institute of Technology, Atlanta, GA 30332-0400

(Dated: February 27, 2017)

We present a $[[7, 1, 3]]$ quantum error-correcting code that is able to achieve fault-tolerant syndrome measurement using one ancillary qubit per stabilizer. All single-qubit Pauli errors on the ancillary qubits propagate to form exclusively correctable errors on the data qubits. We compare the level-1 logical error rates under two noise models: the standard Pauli symmetric depolarizing error model and an anisotropic error model. Fault tolerance cannot be achieved under the standard depolarizing model because errors in two-qubit gates during syndrome extraction can result in logical errors. However, fault tolerance is achievable with an anisotropic error model motivated by control errors that occur on trapped ion qubits. Our results on this $[[7, 1, 3]]$ code demonstrates how physically motivated noise models may simplify fault-tolerent protocols.

arXiv:1702.01155v2 [quant-ph] 24 Feb 2017

I. INTRODUCTION

The operation of a universal quantum computer requires protocols to prevent it from systematic and environmental imperfections. Quantum error-correcting (QEC) [1] codes are among the most promising approaches to deliver scalable and reliable fault-tolerant quantum computation. Topological quantum error correcting codes have a two-dimensional qubit layout that limits qubit interactions to only nearest neighbors, which is suitable for practical implementation using quantum architectures such as superconducting devices and trapped ions [2–4]. Concatenated codes require more resources to be mapped onto local architectures, but can use less resources overall than topological codes for low error rate systems [5]. In general, the optimal choice of quantum error-correcting code is dependent on the actual noise environment and the quantum circuit being used [6]. Many QEC codes, both topological codes and concatenated codes, belong to the family of Calderbank-Shor-Steane (CSS) codes, where X and Z Pauli errors can be treated separately [7, 8].

For a given QEC code, different methods of syndrome extraction, state preparation and decoding can all affect the resulting logical error rate. For syndrome extraction, using a single (bare) ancillary qubit to measure a stabilizer is in general not fault-tolerant, since errors on the ancillary qubitcan propagate to the data and form uncorrectable errors [9, 10]. Although there are various methods to make the syndrome measurement fault-tolerant, these come at the expense of extra resources. Shor's method requires a w-qubit cat state to measure a weight-w stabilizer [11]. An extra qubit is needed to verify the ancillary qubit, but this is not a strict requirement [12, 13]. Steane's method requires the fault-tolerant preparation of a logical state [14], while Knill's method relies on the fault-tolerant preparation of a logical Bell pair [15].

Using bare ancillary qubits for stabilizer measurement can be fault-tolerant if we are guaranteed that single-qubit errors or errors that occur with a probability linearly proportional to the physical error rate do not propagate to form uncorrectable errors. More specifically, if we assume only Pauli errors, then after measuring a stabilizer of weight w a weight $\lfloor w/2 \rfloor$, where $\lfloor x \rfloor$ is the floor of x, error can propagate to the data. This can still be fault-tolerant in several cases. In some codes, the presence of gauge subsystems allow the decomposition of high weight stabilizers into lower weight gauge operators that can be measured in a fault-tolerant fashion using bare ancillary qubits. This is the case of the Bacon-Shor codes [16, 17]. In other cases, codes have a large enough distance such that any error of weight up to $\lfloor w/2 \rfloor$ can be corrected ($d \geq 2\lfloor w/2 \rfloor + 1$). This is the case of large distance surface [3, 18] and color codes [19, 20]. Finally, certain codes with distance $d < 2\lfloor w/2 \rfloor + 1$ allow for stabilizer measurement with bare ancillary qubits because the resulting errors on data qubits are correctable. This is the case for the $[[9, 1, 3]]$ surface code, where the weight-2 errors that propagate when measuring the weight-4 stabilizers are all correctable for specific orderings of the entangling two-qubit gates [21].

In this paper, we present a non-CSS $[[7, 1, 3]]$ QEC code that falls into another category: direct fault-tolerant stabilizer measurement can be achieved because every single-qubit Pauli error on the ancillary qubit propagates to the data to form a correctable error. The code was found by a numerical greedy search for stabilizer codes where single-qubit errors on the ancillary qubits do not lead to a logical error [22]. We refer to this code as the Bare $[[7, 1, 3]]$ code.

Given the guarantee that single-qubit Pauli errors on the ancillary qubits do not lead to logical errors, we want to understand the behavior of the code under higher weight errors. Here we present the results of Monte Carlo stabilizer simulations of the Bare $[[7, 1, 3]]$ code with 3 error correcting steps. We used CHP [23] and a Python-based wrapper to obtain logical error rates for the Bare $[[7, 1, 3]]$ code at the first level of encoding. We also present two alternative Monte Carlo error sampling schemes that we employed in the simulations. We report the logical error rates under two different error models. We find that fault-tolerant syndrome measurement is not achieved under the standard depolarizing error model because, although the code is resilient to any single-qubit error on the ancillary qubit, certain two-qubit errors whose proba-

* ken.brown@chemistry.gatech.edu

bility is linearly proportional to the physical error rate are malignant. Bare ancillary qubits are still fault-tolerant under an anisotropic error model. We report the level-1 pseudothreshold of the code under such error model. In the Appendix we report the level-1 pseudothreshold for two well studied distance-3 quantum error correcting codes: the Steane code [24–26] and the 5-qubit code [27, 28], for comparison.

The paper is organized as follows. Section II introduces the Bare $[[7,1,3]]$ code, and explains how it handles different errors. Section III describes the two noise models under which we study the performance of the Bare $[[7,1,3]]$ code and demonstrates why this error-correcting code is not fault-tolerant under the standard depolarizing noise model. In Section IV, we present the simulation scheme and how the simulation results are used to calculate the pseudothreshold. Section V presents the result obtained from our simulation for the Bare $[[7,1,3]]$ code under two error models.

II. DETAILS OF THE BARE $[[7,1,3]]$ CODE

The Bare $[[7,1,3]]$ code was found through a numerical greedy search of stabilizer codes with the property that single-qubit errors on the bare ancillary qubit would not lead to a logical error. Table I presents the stabilizer generators and logical X and Z operators of the code. As seen from the stabilizers, the code is non-CSS and degenerate.

Stabilizer Generators	Logical Operators
X_0X_4	
X_1X_4	
X_2X_5	$X_L = X_1X_2X_3$
X_3X_6	$Z_L = Z_0Z_1Z_4$
$Z_2Z_3Y_5Y_6$	
$Z_0Z_1Z_2X_3Z_4Z_5$	

TABLE I: List of stabilizers and logical operators X_L, Z_L for the Bare $[[7,1,3]]$ code.

FIG 1 shows the configuration of the stabilizers when the Bare $[[7,1,3]]$ code is embeded in a plane.

A. Single-qubit errors on a bare ancillary qubit

To illustrate how using bare ancillary qubits can lead to uncorrectable errors in some QEC codes, let us consider the $[[7,1,3]]$ Steane code. From Figure 2, we can see that when measuring the stabilizer $X_3X_4X_5X_6$, a single qubit X error on the bare ancillary qubit propagates to form the error X_5X_6 on the data qubits. Although this error is detectable at a later stage, its syndrome is equivalent to an X_0 error. When this correction is applied, the resulting error $X_0X_5X_6$ is equivalent to the logical operator $X_L = X_0X_1X_2X_3X_4X_5X_6$ up to a stabilizer.

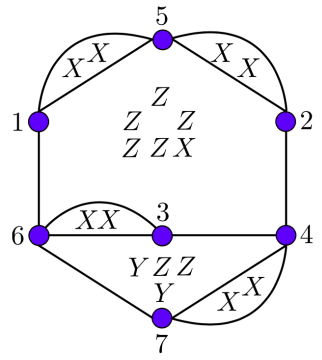

FIG. 1: The Bare $[[7,1,3]]$ code embeded in a plane. Each vertex represents a data qubit, and each stabilizer generator of the code corresponds to a face in this graph.

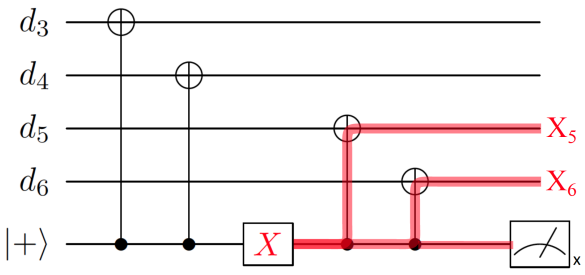

FIG. 2: For the Steane $[[7,1,3]]$ code with bare ancillary qubits, a single-qubit error on the ancillary qubit would lead to a logical error.

On the other hand, in the Bare $[[7,1,3]]$ code, all single-qubit errors on the ancillary qubits propagate to become errors with unique syndromes, hence correctable. This is achieved by considering different schedules for coupling the data to the ancillary qubit when measuring the stabilizers. Note that all ancillary qubits are prepared in the $|+\rangle$ state.

$Z_0 \to 100000$	$X_0 \to 000001$	$Y_0 \to 100001$
$Z_1 \to 010000$	$X_1 \to 000001$	$Y_1 \to 010001$
$Z_2 \to 001000$	$X_2 \to 000011$	$Y_2 \to 001011$
$Z_3 \to 000101$	$X_3 \to 000010$	$Y_3 \to 000111$
$Z_4 \to 110000$	$X_4 \to 000001$	$Y_4 \to 110001$
$Z_5 \to 001010$	$X_5 \to 000011$	$Y_5 \to 001001$
$Z_6 \to 000110$	$X_6 \to 000010$	$Y_6 \to 000100$

TABLE II: Single-qubit error syndromes for the Bare $[[7,1,3]]$ code.

The syndromes for the 21 single-qubit Pauli errors are shown in Table II. Notice that the syndromes of Z_2Z_3 is 001101 which is distinct from all syndromes of single-qubit errors. Similarly, $Z_0Z_2 \to 101000$, $Z_0Z_2X_3 \to 101010$, and $Z_4Z_5 \to 111010$ all have unique syndromes. Since each gate used in a measurement acts between an ancillary qubit and a data qubit where the ancillary qubit controls a Pauli operator on the data qubit, this observation suggests the following syndrome measurement coupling schedule:

1. For each weight-2 generator, the measurement gates can be coupled to the ancillary qubit in any order.

2. For the stabilizer $Z_2Z_3Y_5Y_6$, couple the measurement gates in left-to-right order.

3. For the stabilizer $Z_0Z_1Z_2X_3Z_4Z_5$, couple the measurement gates in order of Z_0, Z_2, X_3, Z_1, Z_4, Z_5.

By using this coupling schedule, for the stabilizer $Z_2Z_3Y_5Y_6$, a single-qubit error on the ancillary qubit can propagate the error Z_2Z_3 onto the data qubits, which has a unique syndrome; for the stabilizer $Z_0Z_1Z_2X_3Z_4Z_5$, a single-qubit error on the ancillary qubit can propagate errors Z_0Z_2, $Z_0Z_2X_3$, and Z_4Z_5 onto the data qubits, which all have unique syndromes. Therefore, all single-qubit errors on the ancillary qubits propagate to exclusively correctable errors.

B. Two-qubit errors on a bare ancillary qubit

Consider the situation where a 2-qubit error occurs on the circuit. Figure 3a illustrates an instance of a 2-qubit Pauli error that can occur under the standard symmetric depolarizing error model. This XX error propagates to become $Z_1X_2X_3Z_4Z_5$, which has syndrome 101011, the same syndrome as $Y_1Z_4Z_5$. Thus, the correction $Y_1Z_4Z_5$ will be applied, and the resulting error is $X_1X_2X_3$, the logical X operator.

The 2-qubit XX error on the control-Y gate propagates to become the error X_5Y_6, which has syndrome 000111, the same as Y_3. After the correction Y_3 is applied, the resulting error $Y_3X_5Y_6$ is equivalent to the logical Z operator up to a stabilizer.

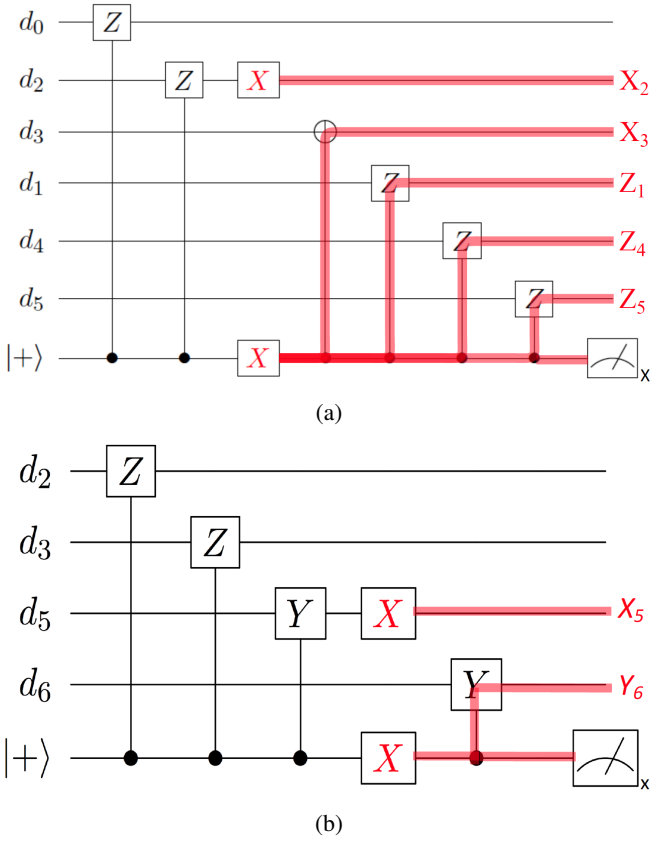

FIG. 3: Two examples of 2-qubit XX errors that propagate to become uncorrectable errors. In (a) the error leads to an X_L, while in (b) the error results in a Z_L.

III. ERROR MODELS

A. Error Models

To study the properties of the Bare $[[7, 1, 3]]$ code, we applied two Pauli error models: the standard depolarizing error model and an anisotropic error model.

1. *Standard Depolarizing Error Model*

The standard depolarizing error model is a common quantum channel where, after each gate, there is a symmetric depolarization with some probability p. After single-qubit gates (including Pauli gates and ancillary qubit preparation gates), a traceless single-qubit Pauli operator, randomly selected from $P = \{X, Y, Z\}$, is applied with probability p_s. After two-qubit gates, a traceless two-qubit Pauli operator, randomly selected from $Q = \{I, X, Y, Z\} \otimes \{I, X, Y, Z\} \backslash \{II\}$, is applied with probablity p_t. Although in general $p_s \neq p_t$, it is common for them to be simulated the same value [15]. A measurement reports the wrong result with probability p_{meas}. For the cases studied here, p_{meas} is set to the single qubit error probability p_s.

2. *Anisotropic Error Model*

For single qubit gates, preparation, and measurement errors remain the same as the standard depolarizing error model. The conceptual motivation for the anisotropic error model is that two-qubit gate errors occur due to errors in the gate coupling. As an example, consider errors in the entangling Mølmer-Sørensen (MS) gate used in trapped ions [29]. The MS gate corresponds to $\exp(-i(\pi/4)XX)$, and an over or under-rortation could result in the coherent error $\exp(-i(\epsilon/2)XX)$, where ϵ denotes the over- or under-rotation angle. For ϵ randomly and symmetrically distributed around 0, this error can be described as a random application of the Pauli error XX with probability p_t, which is determined by the distribution of θ.

The key idea is that the two-qubit correlation in the error is not any two-qubit error, but only the two-qubit Pauli error aligned with the gate. The error after a Control-P gate is then ZP with probability p_t. For the specific case of ion traps, this can be derived from including the single qubit rotations necessary to transform the MS gate into a Control-P gate. In this study, we do not include the individual rotations but work at the level of Control-P gates. We expect random error on the individual qubits in addition to the control error from the two-qubit gate. To account for the random error, after every two-qubit gate we apply the two-qubit anisotropic error with probability p_t followed by single qubit errors with probability p_s on the two-qubits involved in the gate.

B. Fault-tolerance Dependent on Error Model

When studying the behavior of the Bare $[[7, 1, 3]]$ code under the two error models defined in Section III A, we can see that all two-qubit errors in the anisotropic error model can be detected and corrected, because a Z error on the control qubit does not propagate to form other errors on the data. However, for certain two-qubit errors in the standard depolarizing error model, such as the XX error as we have seen in FIG. 3a and FIG. 3b, the errors propagate to become uncorrectable logical errors. Therefore, the Bare $[[7, 1, 3]]$ code can achieve fault-tolerant syndrome measurements under the anisotropic error model because all errors that occur with probability linear in the error rate of physical operations are correctable; however, the code cannot achieve fault-tolerant syndrome measurements under the standard depolarizing error model since certain two-qubit errors that occur with probability linear in the physical error rate propagate to become uncorrectable logical errors.

IV. SIMULATION SCHEME

In this section we present the circuit used in the simulation, the QEC scheme used to perform correction after each round of the Bare $[[7, 1, 3]]$ code with noise, and the calculations we performed to obtain logical error rates. The simulations were done using the CHP stabilizer simulator [23]. The simulation follows the extended rectangle formalism [30] for distance-3 and level-1 encoding.

A. Simulation Circuit

FIG. 4 shows the quantum circuit we constructed to simulate the Bare $[[7, 1, 3]]$ code. The simulated gate is a logical Identity followed by error correction. In the extended rectangle formalism of Ref. [30], the block that we are simulating iss a 1-Rec. The gates are grouped together for each ancillary qubit measurement, and the order of qubit-coupling between the data qubits and ancillary qubits follows exactly the scheduling as required for fault-tolerant measurements of each stabilizer generators: any order for the weight-two generators, Z_2, Z_3, Y_5, Y_6 for $g_5 = IIZZIYY$, and $Z_1, Z_3, X_4, Z_2, Z_5, Z_6$ for $g_6 = ZZZXZZI$. For each gate shown in this circuit, errors of appropriate type are inserted after it with a probability given by the noise model.

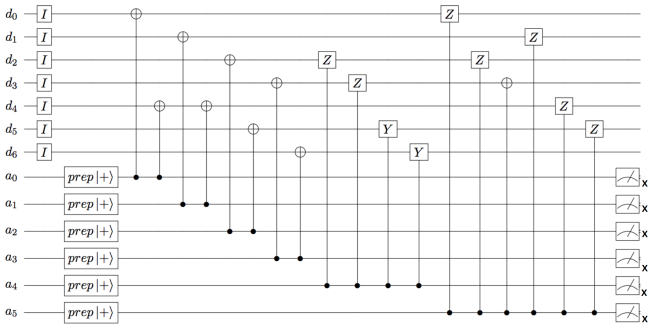

FIG. 4: The circuit simulating the Bare $[[7, 1, 3]]$ code and its measurement steps. The circuit is constructed with only Clifford gates, and errors (single-qubit and two-qubit) are inserted after ancillary qubit preparation, CNOT, Control-Z, Control-Y, and measurements.

The syndrome measurement is repeated up to three times with freshly prepared ancillary qubits. The repetition is necessary due to errors during or between syndrome measurements [31]. If the first two error syndromes agree, correction is performed based on the error syndrome. If the two syndromes disagree, a third syndrome is measured and correction is performed based on the third syndrome.

B. Logical Error Rate Calculation

We calculate the logical error rate under the two different error models for various physical error strengths. At the start of each run of Monte Carlo simulation, we initialize all the data qubits to state $|0\rangle$, and all ancillary qubits to state $|+\rangle$. We then perform one round of noise-free stabilizer measurements to project the state of the data qubits to the logical $|0\rangle$ state. Then the simulation proceeds as follows:

1. Perform the syndrome measurements with random errors inserted using the importance sampling scheme.
2. Apply the decoder to determine the corresponding error configuration.
3. Perform noise-free correction to the final state to project the state back to the codespace.
4. If the final state is different from the initial one, count as one logical error.

In the importance sampling scheme (see Appendix A.2), we classify the error configurations into subsets according

to the number of single- and two-qubit errors present in the configuration. The subset consisting of configurations of s single-qubit errors and t two-qubit errors are labelled by (s, t). For example, if during the execution of the QEC circuit, two single-qubit preparations were faulty and an error occurred after one of the CNOTs, this error configuration belongs to the subset $(2, 1)$.

We perform Monte Carlo simulations on selected error subsets and compute the logical error rate per subset, $p_L(s, t)$, by calculating the ratio of the successful runs over the total number of runs. The total logical error rate, p_L, is calculated as a weighted average over the selected error subsets:

$$p_L(p_s, p_t) = \sum_{s,t} A_{s,t}(p_s, p_t) p_L(s, t),$$

where $A_{s,t}$ is the probability of occurrence of subset (s, t).

We use the calculated logical error rates at different physical error strengths to estimate the pseudothreshold of the code under a particular error model [32]. The pseudothreshold is the intersection between the physical error rate line $y = 2p/3$ and the logical error rate $p_L(p_s, p_t)$. The reason for using this line instead of $y = p$ is that, if we assume a symmetric depolarizing noise model on a single qubit, the infidelity is given by $2p/3$. More intuitively, if we focus on a single-qubit Pauli state, like $|0\rangle$, only two Pauli errors (X and Y in this case) will cause an error. Furthermore, this will result in a slightly more pessimistic value for the pseudothreshold.

V. RESULTS

In this section we present and analyze the results from numerical Monte Carlo simulations of the Bare $[[7, 1, 3]]$ code under different noise models. We first focus on the standard depolarizing error model and then on the anisotropic error model. We show that the Bare $[[7, 1, 3]]$ code does not have a pseudothreshold under the standard depolarizing error model, due to some uncorrectable two-qubit errors that have probability linear in the physical error strength.

A. Standard Depolarizing Error Model

FIG. 5 presents the logical error rates for the standard depolarizing model with $p_s = p_t = p$ for several values of p. The best fit corresponds to a function with a linear term.

Although there is an intersection between the logical error rate and the physical error rate, the curves still remain parallel for physical error rates below the intersection. The fact that there is still a linear term in the logical error rate implies that we would not observe an exponential suppression on the logical error rate with subsequent levels of concatenation. Thus, this intersection is not a pseudothreshold for the Bare $[[7, 1, 3]]$ code, and the code is not fault-tolerant under the standard depolarizing error model. Examples of why this would happen were shown in FIG. 3.

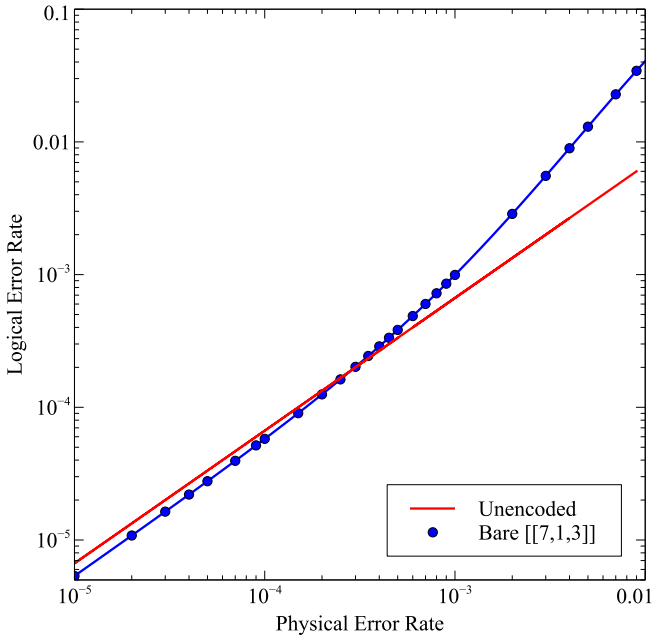

FIG. 5: Logical error rate plot for the Bare $[[7, 1, 3]]$ code under the standard error model. The logical error rate of the code remains parallel to the physical line for physical error rates below the intersection indicates that the error-correction under standard model fails for a single error.

B. Anisotropic Error Model

We now calculate the pseudothreshold of the Bare $[[7, 1, 3]]$ code under the anisotropic error mode. In this model, the physical error strength after each gate is p, and $p_s = p_t = p$. By performing a quadratic fit for the logical error rates under the anisotropic error model and computing the intersection of the fitting curve with the physical error rate, we obtain a pseudothreshold for the Bare $[[7, 1, 3]]$ code. This is because all single-qubit and two-qubit errors that occur with probability linear in p are guaranteed to be detected and corrected by the Bare $[[7, 1, 3]]$ code. From FIG. 6 we can see that the pseudothreshold occurs at 2.0×10^{-4}.

C. Comparison of Results for $p_s \ll p_t$

Since the two-qubit errors are the sources of logical errors, here we compare the results under the two error models with two-qubit errors the dominating errors in the circuit.
In FIG. 7, we compare the performances of the Bare $[[7, 1, 3]]$ code under the two error models, with $p_t = 1000 \times p_s$. The pseudothreshold of the Bare $[[7, 1, 3]]$ code under the

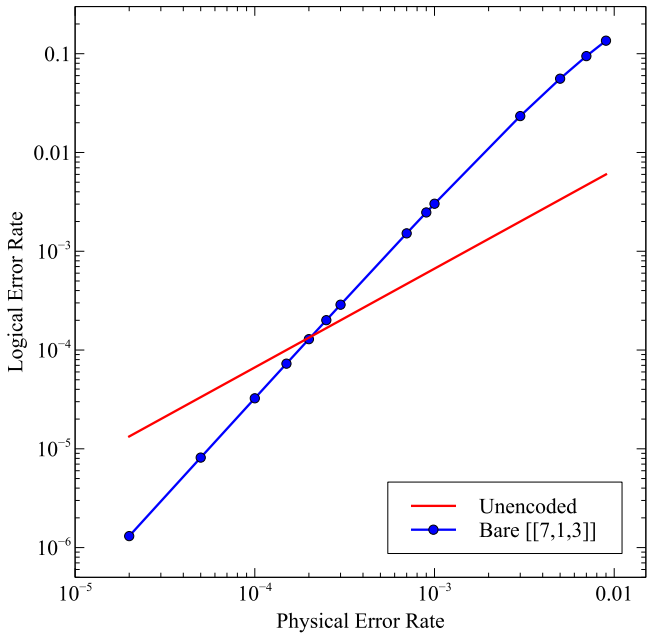

FIG. 6: Pseudothreshold plot for the Bare $[[7,1,3]]$ code under the anisotropic error model, $p_s = p_t$. The pseudothreshold is at $p = 2.0 \times 10^{-4}$. The Bare $[[7,1,3]]$ code is fault-tolerant under the anisotropic error model.

anisotropic error model in this case occurs at $p_t = 1.2 \times 10^{-3}$. Since now the two-qubit errors dominate all error configurations, and there are only three types of two-qubit errors, the resulting pseudothreshold of the Bare $[[7,1,3]]$ code is higher than in the case of $p_s = p_t$. Similar to the $p_t = p_s$ case, there is no clear pseudothreshold for the standard depolaring error model.

VI. CONCLUSIONS

In this paper we have presented properties of a new $[[7,1,3]]$ stabilizer code that can achieve fault-tolerant syndrome extractions using a single ancillary qubit under the anisotropic error model, and showed why certain two-qubit errors under the standard depolarizing error model would prevent this code from achieving fault-tolerant measurements. In particular, the limit on total number of syndrome outcomes makes it impossible for the lookup table decoder to detect and correct all two-qubit errors in the standard depolarizing error model. Overall, the Bare $[[7,1,3]]$ code shows better performance under realistic error models. We note that the $[[7,1,3]]$ triangle code presented in [4] also uses a single ancillary qubit per stabilizer for syndrome extraction and is able to achieve fault-tolerance.

A direction of future work could be to study the behavior of the Bare $[[7,1,3]]$ code under realistic error models such as decoherence and amplitude damping, and tailor this code for architecture-specific noise environments where limitations on

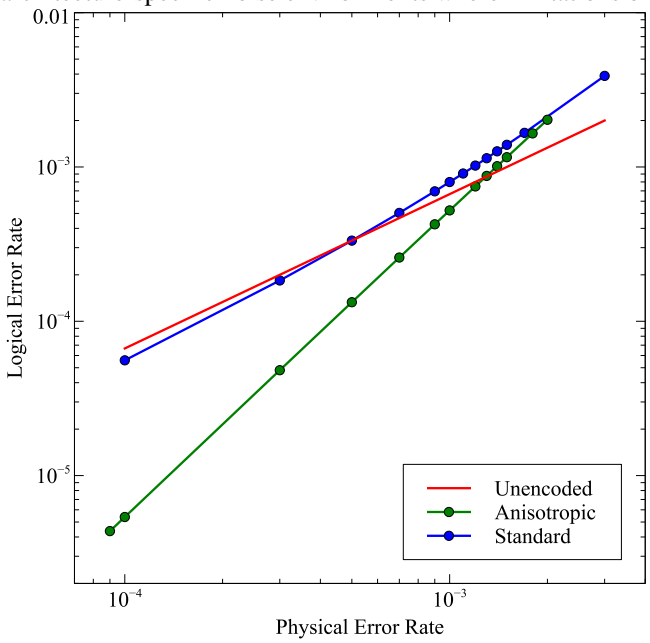

[ht]

FIG. 7: Comparison of logical error rate for the Bare $[[7,1,3]]$ code under the standard depolarizing error model and the anisotropic error model, with $p_t = 1000 p_s$. There is a clear pseudothreshold for the anisotropic error model at $p_t = 1.2 \times 10^{-3}$, but no pseudothreshold for the standard depolaring error model.

ancillary qubit resources and measurement times are required. The fact that the Bare $[[7,1,3]]$ code does not perform well under the theoretical standard error model but can achieve fault-tolerant measurements under a more realistic error model suggests that more effort should be put into designing and finding error correcting codes that help achieve fault-tolerant quantum computation under realistic scenarios. As realistic error models are becoming more and more relevant, development of environment-specific error correcting codes will become more important.

ACKNOWLEDGMENTS

This work would not have been possible without the help of Andrew Cross. We would like to thank him for discovering this code, for encouraging us to study its properties, and for discussions and comments on the manuscript. We thank Colin Trout for comments on the manuscript and for his help with the figures. This work was supported by the Office of the Director of National Intelligence - Intelligence Advanced Research Projects Activity through ARO contract W911NF-10-1-0231 and the National Science Foundation grant PHY-1415461.

[1] P. W. Shor, Phys. Rev. A **52**, R2493 (1995).
[2] R. Raussendorf and J. Harrington, Phys. Rev. Lett. **98**, 190504 (2007).
[3] A. G. Fowler, A. M. Stephens, and P. Groszkowski, Phys. Rev. A **80**, 052312 (2009).
[4] T. J. Yoder and I. H. Kim, arXiv preprint arXiv:1612.04795 (2016).
[5] K. M. Svore, D. P. Divincenzo, and B. M. Terhal, Quantum Info. Comput. **7**, 297 (2007).
[6] M. Suchara, A. Faruque, C. Y. Lai, G. Paz, F. T. Chong, and J. Kubiatowicz, in *In Proceedings of IEEE International Conference on Computer Design* (IEEE, 2013), pp. 419–426.
[7] A. Steane, Proceedings: Mathematical, Physical and Engineering Sciences **452**, 2551 (1996).
[8] A. R. Calderbank and P. W. Shor, Phys. Rev. A **54**, 1098 (1996).
[9] M. A. Nielsen and I. L. Chuang, *Quantum computation and quantum information* (Cambridge university press, 2010).
[10] J. Preskill, in *Introduction to quantum computation and information* (Singapore: World Scientific, 1998), pp. 213–269.
[11] P. W. Shor, in *Foundations of Computer Science, 1996. Proceedings., 37th Annual Symposium on* (IEEE, 1996), pp. 56–65.
[12] D. P. DiVincenzo and P. Aliferis, Phys. Rev. Lett. **98**, 020501 (2007).
[13] Y. Tomita, M. Gutiérrez, C. Kabytayev, K. R. Brown, M. R. Hutsel, A. P. Morris, K. E. Stevens, and G. Mohler, Phys. Rev. A **88**, 042336 (2013).
[14] A. M. Steane, Phys. Rev. Lett. **78**, 2252 (1997).
[15] E. Knill, Nature **434**, 39 (2005).
[16] D. Bacon, Phys. Rev. A **73**, 012340 (2006).
[17] P. Aliferis and A. W. Cross, Phys. Rev. Lett. **98**, 220502 (2007).
[18] A. G. Fowler, M. Mariantoni, J. M. Martinis, and A. N. Cleland, Phys. Rev. A **86**, 032324 (2012).
[19] H. Bombin and M. A. Martin Delgado, Phys. Rev. Lett. **97**, 180501 (2006).
[20] A. J. Landahl, J. T. Anderson, and P. R. Rice, arXiv:1108.5738 [quantph] (2011).
[21] Y. Tomita and K. M. Svore, Phys. Rev. A **90**, 062320 (2014).
[22] A. Cross, Personal Communication (2016).
[23] S. Aaronson and D. Gottesman, Phys. Rev. A **70**, 052328 (2004).
[24] A. M. Steane, Phys. Rev. Lett. **77**, 793 (1996).
[25] M. Gutiérrez and K. R. Brown, Phys. Rev. A **91**, 022335 (2015).
[26] M. Gutiérrez, C. Smith, L. Lulushi, S. Janardan, and K. R. Brown, Phys. Rev. A **94**, 042338 (2016).
[27] D. P. DiVincenzo and P. W. Shor, Phys. Rev. Lett. **77**, 3260 (1996).
[28] C. H. Bennett, D. P. DiVincenzo, J. A. Smolin, and W. K. Wootters, Phys. Rev. A **54**, 3824 (1996).
[29] A. Sørensen and K. Mølmer, Phys. Rev. Lett. **82**, 1971 (1999).
[30] P. Aliferis, D. Gottesman, and J. Preskill, Quantum Info. Comput. **6**, 97 (2006).
[31] F. J. MacWilliams and N. J. A. Sloane, *The theory of error correcting codes* (Elsevier, 1977).
[32] K. M. Svore, A. W. Cross, I. L. Chuang, and A. V. Aho, Quantum Information and Computation **6**, 193 (2006).
[33] S. Janardan, Y. Tomita, M. Gutiérrez, and K. R. Brown, Quantum Information Processing **15**, 3065 3079 (2016).
[34] S. Bravyi and A. Vargo, Phys. Rev. A **88**, 062308 (2013).

Appendix A: Efficient Sampling Algorithm for Monte Carlo Simulations

For a given QEC circuit and a physical noise model, obtaining an exact algebraic expression for the logical error rate is in principle possible. In the context of a stabilizer code and a noise model consisting of stochastic discrete errors, this amounts to (1) enumerating every possible error configuration on the circuit, (2) calculating its probability of occurrence, and (3) determining whether or nor it results in a logical error. The logical error rate is then given by:

$$p_L = \sum_{i=0}^{N_c} A_i \, p_i, \tag{A1}$$

where N_c is the total number of error configurations, A_i is the probability of occurrence of error configuration i, and $p_i = 0(1)$ if the error configuration i is correctable (uncorrectable). Although possible in principle, the exact computation of a logical error rate is infeasible in practice, due to the high cardinality of the error configuration set. For a circuit with n_g gates and s possible different errors after each gate, $N_c = (s+1)^{n_g}$. Even a modest circuit, like a level-1 QEC routine for a distance-3 code consisting of 3 rounds of stabilizer measurements, contains more than 100 gates and making the exact computation of the logical error rate impractical.

It is, therefore, common to employ Monte Carlo methods to estimate p_L [2, 3, 15, 33]. The basic procedure to obtain a logical error rate consists of two steps: (1) the generation of a faulty circuit (an error configuration) based on the physical noise model and (2) the simulation of the circuit to determine if that particular error configuration is correctable. In this section, we describe the two different Monte Carlo methods used in the first step. The first one utilizes traditional direct sampling of the whole error configuration set. The second one relies on importance sampling of the error configuration subsets that are relevant to the logical error rate. Both methods are based on direct sampling, i.e., each error configuration is completely uncorrelated from the previous ones.

1. Traditional Sampler

To generate an error configuration, the traditional sampler traverses the circuit exhaustively and after each gate an error is inserted with a probability given by the noise model. This approach is convenient for high error rates. However, it is problematic if the error rate is low, because most of the times no error is inserted. For illustrative purposes, consider a simple case where the error rate $p = 0.1\%$ is the same for ech gate and the circuit has $N_g = 100$ gates. The traditional sampler will return an error-free circuit $(1-p)^{n_g} \approx 90\%$ of the runs. Furthermore, if the circuit corresponds to a fault-tolerant QEC

protocol of a distance-3 code, by construction no error configuration of weight-1 will result in a logical error. This implies that $(1-p)^{n_g} + n_g p(1-p)^{n_g-1} \approx 99.5\%$ of the runs will generate an error configuration which is known a priori to be correctable. The limitation of the traditional sampler becomes even more dramatic for lower error rates and codes of higher distance [34].

2. Importance Sampler

It is possible to split the error configuration set into subsets based on each configuration's error weight (number of errors). The key advantage of the importance sampler relies on two features of this particular subset splitting: (1) it is straightforward to compute analytically the total probability of occurrence of each subset (the sum of the probabilities of occurrence of the error configurations in the subset) and (2) for low error rates we can safely ignore high weight error subsets, since their probability of occurrence will be vanishingly small.

Here we consider subsets in terms of both errors that occur after single-qubit gates and two-qubit gates. For example, a subset labelled by (s,t) contains all error configurations of the circuit with s errors after single-qubit gates and t errors after two-qubit gates. Notice that an error after a two-qubit gate can still be of weight 1. Let n_s and n_t be the total number of single-qubit gates and two-qubit gates in this circuit. We assume an error model where the error probability is the same for all single-qubit gates (p_s) and the error probability is also the same for all two-qubit gates (p_t). The probability of occurrence of the error subset (s,t) is then:

$$A_{s,t}(p_s,p_t) = \binom{n_s}{s} p_s^s (1-p_s)^{n_s-s} \binom{n_t}{t} p_t^t (1-p_t)^{n_t-t}. \tag{A2}$$

Given a quantum circuit and a noise model, the algorithm to estimate the logical error rate using the importance sampler consists of three steps:

1. Select a tolerance value. This corresponds to the total added probability of occurrence of the high weight subsets that will not be sampled. In the worst scenario imaginable, every error configuration in the excluded subsets would result in a logical error. The tolerance value represents the worst-case discrepancy between the real and the obtained logical error rate. In particular, it provides a worst-case upper bound to the logical error rate.

2. For each error subset (s,t), use direct Monte Carlo sampling to approximate its logical error rate $p_L(s,t)$. The sampling is done by randomly selecting s single-qubit gates and t two-qubit gates and adding errors after them.
3. Calculate the total logical error rate for the circuit:

$$p_L(p_s,p_t) = \sum_{s,t} A_{s,t}(p_s,p_t) p_L(s,t), \tag{A3}$$

where $A_{s,t}(p_s,p_t)$ is computed analytically using Equation A2.

Notice that the logical error rate $p_L(s,t)$ for a particular (s,t) subset is not a function of the physical error rates p_s and p_t. This means that, for a given circuit and noise model, we can pre-compute the logical error rate for each relevant subset, and use those values to evaluate the total logical error rate for different physical error rates. In contrast to the traditional sampler, there is no need to re-run the Monte Carlo simulations for different values of p_s and p_t. We simply calculate new values for the probabilities of subset occurrence $A_{s,t}$ and compute p_L using Equation A3. Once the Monte Carlo simulations for each relevant subset are done, the logical error rates for different physical error rates can be computed at no additional cost, making the importance sampler much more efficient than the traditional one. However, for high physical error rates (about 10^{-2} and higher) the importance sampler becomes either inaccurate or very slow. The trade-off arises because as the error rate increases so does the probability of occurrence of higher weight subsets and therefore the number of subsets that need to be included to obtain an accurate result. In this error regime, it is suitable to employ the traditional sampler.

3. Comparing Performance of Sampling Algorithms

In order to test the performance of the importance sampler, we simulated the logical error rate for the Steane $[[7,1,3]]$ code, the five-qubit code, and the Bare $[[7,1,3]]$ code with both the traditional and the importance sampling algorithm. To make sure that the results of the two sampling algorithms are comparable, we analytically proved that the probability for an arbitrary error to occur at any location in the circuit is the same for both sampling algorithms.
From both FIG. 8 and FIG. 9 we can see that the results of the two sampling algorithms coincide exactly at lower physical error rates, but can start to diverge as physical error rate increases, with the logical error rate obtained from the traditional sampler slightly higher than that from the importance sampler. This is because for a given number of subsets, at lower physical error rates these subsets are enough to calculate the cumulative logical error rate to a high accuracy, but for higher physical error rates the importance sampler requires to sample a larger number of error subsets in order to achieve the same level of accuracy in cumulative logical error rate. In this case, the traditional sampler accounts for all error subsets of this circuit, while the importance sampler only accounts for a small number of subsets, hence lead to a smaller logical error rate.

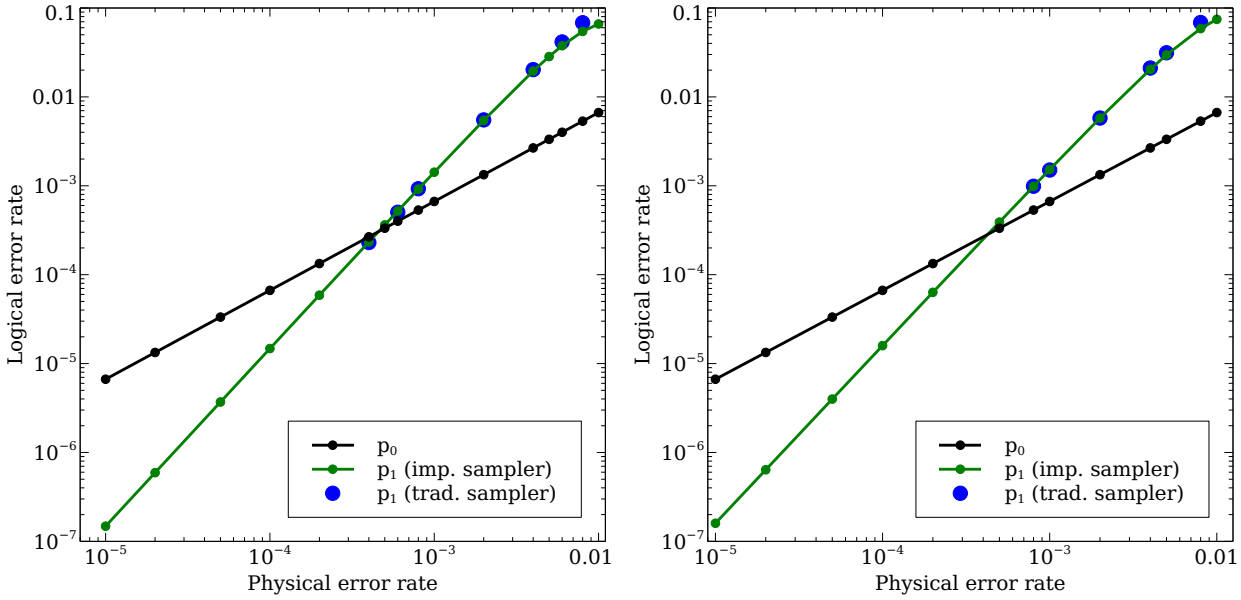

(a) Steane $[[7, 1, 3]]$ code

(b) Five-qubit code

FIG. 8: Simulated logical error rate for the Steane $[[7, 1, 3]]$ code and the five-qubit code with Shor-style ancillary qubits under the standard depolarizing error model.

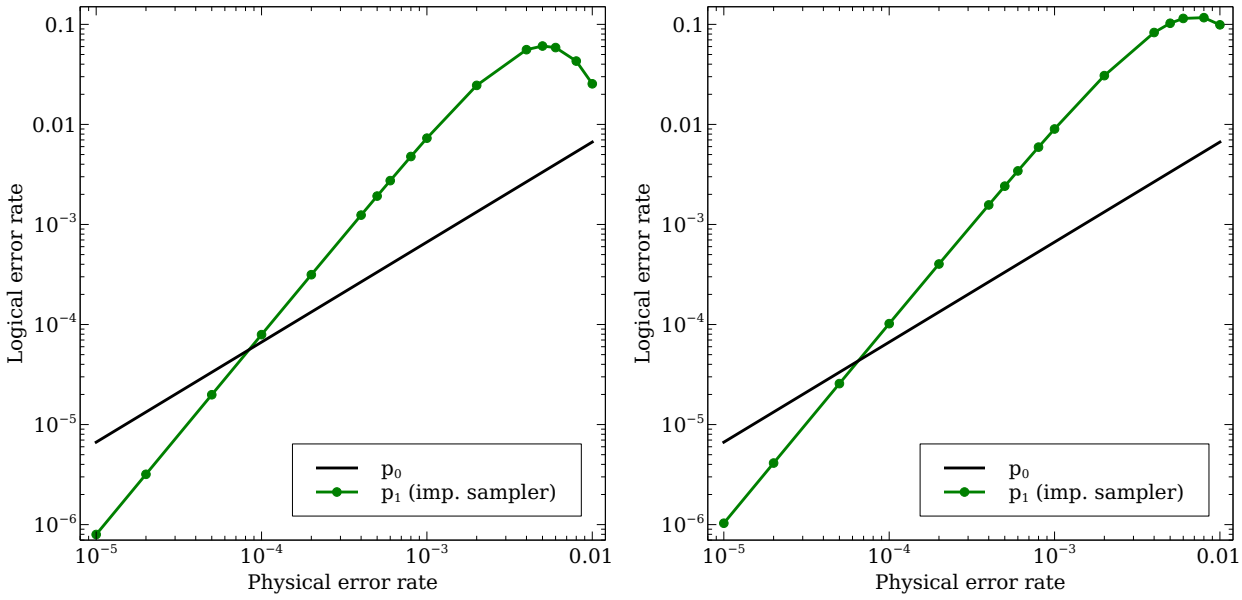

(a) Steane $[[7, 1, 3]]$ code

(b) Five-qubit code

FIG. 9: Simulated logical error rate for the Steane $[[7, 1, 3]]$ code and the five qubit code with Shor-style ancillary qubits under the anisotropic error model.